



# Colorado geoid computation experiment: overview and summary

Yan Ming Wang<sup>1</sup> · Laura Sánchez<sup>2</sup> · Jonas Ågren<sup>3,4,5</sup> · Jianliang Huang<sup>6</sup> · René Forsberg<sup>7</sup> · Hussein A. Abd-Elmotaal<sup>8</sup> · Kevin Ahlgren<sup>1</sup> · Riccardo Barzaghi<sup>9</sup> · Tomislav Bašić<sup>10</sup> · Daniela Carrion<sup>9</sup> · Sten Claessens<sup>11</sup> · Bihter Erol<sup>12</sup> · Serdar Erol<sup>12</sup> · Mick Filmer<sup>11</sup> · Vassilios N. Grigoriadis<sup>13</sup> · Mustafa Serkan Isik<sup>12</sup> · Tao Jiang<sup>14</sup> · Öykü Koç<sup>12</sup> · Jordan Krcmaric<sup>1</sup> · Xiaopeng Li<sup>1</sup> · Qing Liu<sup>2</sup> · Koji Matsuo<sup>15</sup> · Dimitris A. Natsiopoulou<sup>13</sup> · Pavel Novák<sup>16</sup> · Roland Pail<sup>17</sup> · Martin Pitoňák<sup>16</sup> · Michael Schmidt<sup>2</sup> · Matej Varga<sup>18</sup> · Georgios S. Vergos<sup>13</sup> · Marc Véronneau<sup>6</sup> · Martin Willberg<sup>17</sup> · Philipp Zingerle<sup>17</sup>

Received: 13 April 2020 / Accepted: 16 September 2021

This is a U.S. government work and not under copyright protection in the U.S.; foreign copyright protection may apply 2021

## Abstract

The primary objective of the 1-cm geoid experiment in Colorado (USA) is to compare the numerous geoid computation methods used by different groups around the world. This is intended to lay the foundations for tuning computation methods to achieve the sought after 1-cm accuracy, and also evaluate how this accuracy may be robustly assessed. In this experiment, (quasi)geoid models were computed using the same input data provided by the US National Geodetic Survey (NGS), but using different methodologies. The rugged mountainous study area (730 km × 560 km) in Colorado was chosen so as to accentuate any differences between the methodologies, and to take advantage of newly collected GPS/leveling data of the Geoid Slope Validation Survey 2017 (GSVS17) which are now available to be used as an accurate and independent test dataset. Fourteen groups from fourteen countries submitted a gravimetric geoid and a quasigeoid model in a 1' × 1' grid for the study area, as well as geoid heights, height anomalies, and geopotential values at the 223 GSVS17 marks. This paper concentrates on the quasigeoid model comparison and evaluation, while the geopotential value investigations are presented as a separate paper (Sánchez et al. in *J Geodesy* 95(3):1. <https://doi.org/10.1007/s00190-021-01481-0>, 2021). Three comparisons are performed: the area comparison to show the model precision, the comparison with the GSVS17 data to estimate the relative accuracy of the models, and the differential quasigeoid (slope) comparison with GSVS17 to assess the relative accuracy of the height anomalies at different baseline lengths. The results show that the precision of the 1' × 1' models over the complete area is about 2 cm, while the accuracy estimates along the GSVS17 profile range from 1.2 cm to 3.4 cm. Considering that the GSVS17 does not pass the roughest terrain, we estimate that the quasigeoid can be computed with an accuracy of ~2 cm in Colorado. The slope comparisons show that RMS values of the differences vary from 2 to 8 cm in all baseline lengths. Although the 2-cm precision and 2-cm relative accuracy have been estimated in such a rugged region, the experiment has not reached the 1-cm accuracy goal. At this point, the different accuracy estimates are not a proof of the superiority of one methodology over another because the model precision and accuracy of the GSVS17-derived height anomalies are at a similar level. It appears that the differences are not primarily caused by differences in theory, but that they originate mostly from numerical computations and/or data processing techniques. Consequently, recommendations to improve the model precision toward the 1-cm accuracy are also given in this paper.

**Keywords** Colorado experiment · 1-cm geoid experiment · Geoid computation · Quasigeoid computation · Geoid-quasigeoid separation term · GRAV-D · GSVS17 · GPS/leveling

## Abbreviations

AUTH Aristotle University of Thessaloniki, Greece

✉ Yan Ming Wang  
Yan.Wang@noaa.gov

CASM

Chinese Academy of Surveying and Mapping, China

CGS

Canadian Geodetic Survey, Canada

Curtin

Curtin University, Australia

DGFI

Deutsches Geodätisches Forschungsinstitut, Technical University of Munich, Germany

Extended author information available on the last page of the article

DTU	Technical University of Denmark, Denmark
Minia	Minia University, Egypt
NGS	US National Geodetic Survey, NOAA, USA
GSI	Geospatial Information Authority of Japan, Japan
IAPG	Institute for Astronomical and Physical Geodesy, Technical University of Munich, Germany
ITU	Istanbul Technical University, Turkey
KTH	University of Gävle, Lantmäteriet, Royal Institute of Technology, Sweden
NTIS-GEOF	New Technologies for the Information Society, University of West Bohemia, Czech Republic & University of Zagreb, Croatia
Polimi	Politecnico di Milano, Italy

## 1 Introduction

According to Resolution No. 1, 2015 of the International Association of Geodesy (IAG, Drewes et al. 2016, p. 981), the International Height Reference System (IHRs, Ihde et al. 2017) is defined in terms of geopotential numbers  $C_P = W_0 - W_P$ , where  $W_P$  is the geopotential at a point of interest  $P$ , and  $W_0 = 62\,636\,853.4 \text{ m}^2 \text{ s}^{-2}$  (Sánchez et al. 2016) as adopted by the IAG as the reference level for the IHRs. Since the  $W_0$  value is conventionally fixed, the primary value to be determined is the potential value  $W_P$ . As absolute potential values cannot be measured directly, the value  $W_P$  is to be determined from observable gravity field data by applying appropriate geoid or quasigeoid determination methods. In the (quasi)geoid computations, the primary quantity to be determined is the disturbing potential  $T = W - U$ , which is the difference between the actual gravity potential  $W$  and the normal gravity potential  $U$  generated by the adopted reference ellipsoid. Once  $T_P$  is computed, the determination of  $W_P$  is straightforward. However, the estimated value of the disturbing potential relies not only on available gravity data but also on gravity field modeling approaches. This includes different methods for handling terrain effects, filtering and combining gravity data, treating long-wavelength errors, formulating mathematical models to continue and transform gravity data and terrain effects, etc. Since there is no standardization in the computation of the disturbing potential and there are many parameter choices when handling gravity and terrain data, potential values estimated by different methods inevitably differ. Thus, different groups can generate quite different (quasi)geoid models from the same input gravity data.

To assess how much the results depend on applied computation methods, fourteen groups from thirteen countries working on regional geoid modeling agreed in August 2017 to determine geoid heights, height anomalies and geopoten-

tial values using the same input data and their own modeling strategies. For this purpose, NGS provided GPS/leveling data, terrestrial and airborne gravity data, and a digital terrain model for a test area of about  $730 \text{ km} \times 560 \text{ km}$  in Colorado, USA. From 2018 to 2020, about 30 geodesists specialized in (quasi)geoid determination performed iterative computations of local (quasi)geoid models using these data, identifying their discrepancies and homogenizing to a large extent their different processing strategies. This initiative was successful in that the final models presented an agreement of around 2 cm in terms of the standard deviation of their differences. The contributing solutions represent the state-of-the-art in precise high-resolution gravity field modeling. The results of this experiment provide a benchmark for calibration of regional gravity field modeling methods and provide a basis for evaluation and further development of strategies and procedures to increase the achievable accuracy in determination of the regional gravimetric (quasi)geoid.

This paper describes key aspects of this joint international effort known as the Colorado 1-cm geoid experiment. The basic processing requirements agreed for the computation of the geoid and quasigeoid models are given in the Appendix. Section 2 describes the gravity data, the digital elevation model, and the GPS/leveling data provided by NGS for the Colorado experiment as well as the global geopotential models (GGM) used as a reference field in the (quasi)geoid modeling. Section 3 presents the key aspects of the computation methods applied by the different groups. The comparison of estimated quasigeoid models is shown and analyzed in Sect. 4; the comparison of potential values as the International Height Reference Frame coordinates is discussed in Sánchez et al. (2021). Finally, Sect. 5 discusses the main findings of the 1-cm geoid experiment and sets out recommendations for future research.

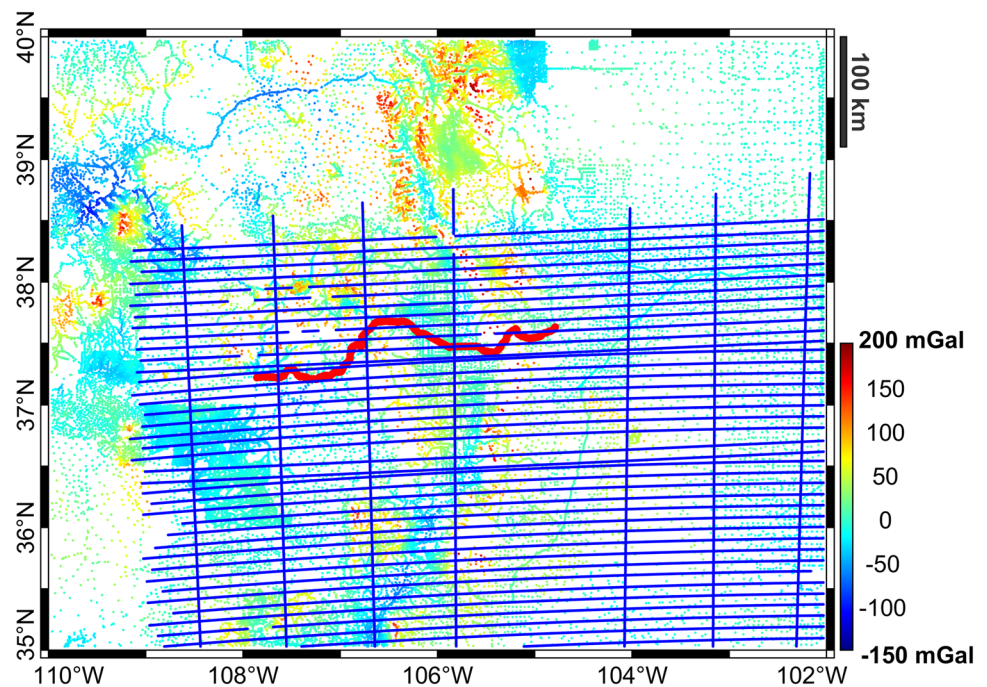
## 2 Input data for the Colorado 1-cm geoid experiment

The following datasets were provided for the Colorado experiment:

### 2.1 Terrestrial and GRAV-D airborne gravity datasets

The terrestrial gravity data cover an area bordered by latitude  $35^\circ \text{ N}$  to  $40^\circ \text{ N}$  and longitude  $110^\circ \text{ W}$  to  $102^\circ \text{ W}$ , see Fig. 1. This dataset combines the US National Geospatial Intelligence Agency and NGS terrestrial gravity data and contains 59,303 gravity observations. Additionally, airborne gravity data from NGS's GRAV-D project were provided (Damiani et al. 2017). Data from the survey block MS05 were debiased using the maximum median technique (Wang et al. 2017a), and then resampled at 1 Hz. The gravity observa-

**Fig. 1** Distribution of terrestrial and GRAV-D gravity observations. The straight lines (in blue) represent the GRAV-D airborne gravity at flight altitude. The GSVS17 profile (purple curve) is along US Highway 160 from Durango to Walsenburg. These data were provided as observed gravity values, which the different participants had to convert to gravity anomalies using their own methods. The color ramp represents the free-air gravity anomaly



tions are given at flight altitude ( $\sim 6,000$  m) with positions in the IGS08 reference frame (Reischung et al. 2012).

Figure 1 shows the spatial distribution of the terrestrial and airborne gravity throughout the region. Sparse distribution of terrestrial gravity data is seen in the northern and southwestern parts of the region along with the most easterly segment of the GSVS17 profile (see  $\sim 105.5^\circ\text{W}$ ). Statistics of the terrestrial and airborne gravity data are summarized in Table 1. In general, the airborne data have uniform coverage and consistent quality, while the surface data contain outliers and have variable spatial coverage.

## 2.2 Digital elevation model: SRTM v4. 1

The SRTM v4.1 data (Jarvis et al. 2008) were provided as a 3'' resolution model throughout the region (Fig. 2). The topographic heights are fixed for spikes and voids (Ahlgren et al. 2018). Some groups also utilized the topographic potential models  $dV\_ell\_Earth2014$  (herein called Earth2014) (Rexer et al. 2016) and ERTM2160 (Hirt et al. 2014), which are based on the same SRTM data.

## 2.3 GPS/leveling data sets

Two GPS/leveling data sets were used in the experiment. The first set corresponds to NAVD88 benchmarks with GPS observations. These data are quite old with over half of the GPS observations collected in the 1990s, while the leveling lines were observed more sporadically over the last century with most of the data being observed in the 1930s and 1980s. There is no accuracy estimated for the GPS/leveling data-

derived height anomalies. However, the comparison results of this experiment indicate a 5 cm accuracy (relative). This data set was distributed to the contributing groups with the intention that it was used as initial reference for the quality control in the (quasi)geoid computations. The original ellipsoidal height was in the NAD83 system, but it was converted to the IGS08 frame for this experiment. Out of 509 benchmarks, 467 benchmarks were from the NGS Integrated Database and the rest from the NGS OPUS-Share Tool (<https://www.ngs.noaa.gov/OPUS/>). The spatial distribution of the benchmarks is sparse due to the mountainous terrain (see Fig. 2).

The second data set is from the GSVS17 survey in the IGS08 frame. GPS, leveling, gravity and astrogeodetic deflections of the vertical were observed at 223 marks spaced at about 1.6 km along Highway US 160 from Durango to Walsenburg in the summer of 2017 (van Westrum et al. 2021). The accuracy of the geoid undulations ( $N_{GSVS17} = h_{GPS} - H_{lev}$ ) inferred from the GPS-based ellipsoidal heights  $h_{GPS}$  and the leveling-based orthometric heights  $H_{lev}$  is estimated to be around 1.5 cm between the marks (ibid.). The accuracy of the GSVS17 height anomalies ( $\zeta_{GSVS17} = h_{GPS} - H^N$ ), where  $H^N$  is the normal height computed from the adjusted geopotential numbers of GSVS17, is estimated as 1.2 cm (see Sect. 4.3). The GSVS17 dataset was not made available to any of the contributing groups (including NGS) and used only as an independent, final comparison.

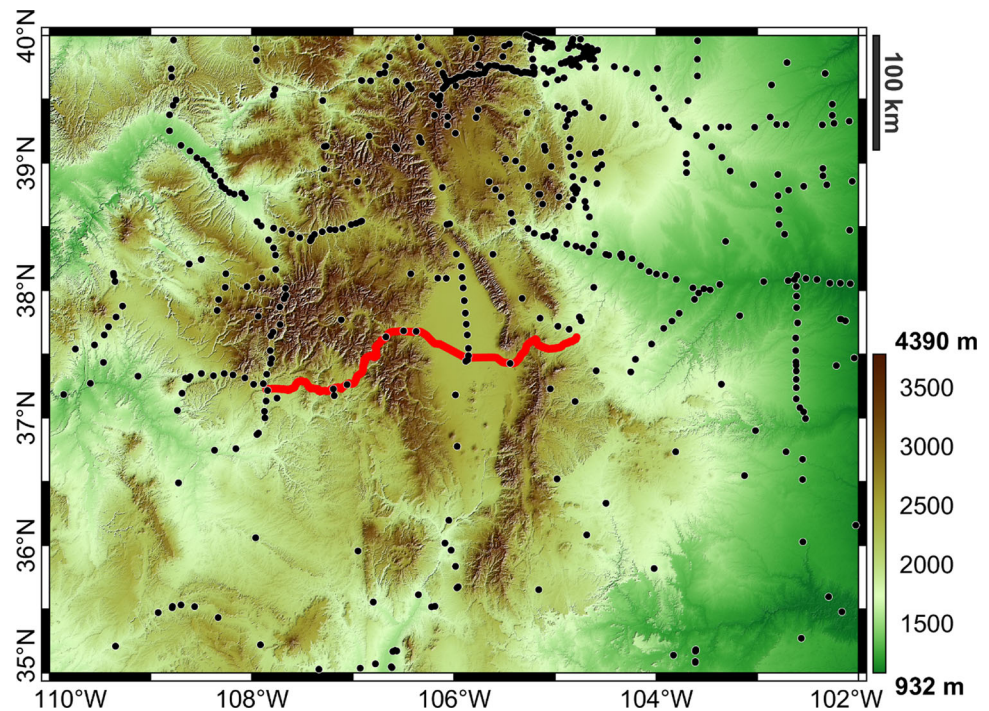
## 2.4 Global geopotential models (GGMs)

It was specified that three different GGMs could be used as reference models in the (quasi)geoid computations (Sánchez

**Table 1** Statistics of the input gravity data

	Terrestrial (59,303 observations)		Airborne (283,716 observations)	
	Free-air gravity anomaly (mGal)	Orthometric height (m)	Free-air gravity disturbance (mGal)	Ellipsoidal height (m)
Mean	5.3	2134	5.7	6186
STD	38.2	577	29.0	695
RMS	38.5	2201	29.5	6225
Min	-165.7	950	-45.6	5209
Max	211.9	4399	123.5	7905

**Fig. 2** Topographic heights based on SRTM v4.1 (Jarvis et al. 2008) model in the Colorado area with a spatial resolution of 3 arc-second. The heights have a mean value of 2,017 m and a standard deviation (STD) of 614 m. The minimum height is 932 m and the highest peak is 4385 m. The red line represents the GSVS17 profile along US Highway 160 from Durango to Walsenburg. The black dots show the distribution of the GPS/leveling data provided to the group



et al. 2018): xGEOID17REFB (herein called RefB) d/o 2190 (Wang et al. 2017a), XGM2016 d/o 719 (Pail et al. 2017; 2018), and GOCO05S d/o 280 (Mayer-Gürr et al. 2015). It was thus up to the particular geoid modeler to decide whether to use a satellite-only or a combined GGM. All three GGMs are given in the zero-tide system.

### 3 Key characteristics of the computation methods contributing to the Colorado experiment

The computation methodologies are roughly classified according to the geodetic boundary-value problems (GBVPs). Eleven groups computed quasigeoid models under the scalar-free Molodensky GBVP (e.g., Molodensky et al. 1962; Hofmann-Wellenhof and Moritz 2005; Moritz 1980) and the fixed GBVP (e.g., Koch and Pope 1972; Heck 2011). Three groups computed the geoid based on the scalar-free

Stokes GBVP (e.g., Vaníček and Martinec 1994; Huang and Véronneau 2013; Abd-Elmotaal and Kühtreiber 2003, 2021), then converted geoid undulations into height anomalies using the geoid-quasigeoid separation term. Most of the solutions applied the remove-compute-restore (RCR) technique using different parameters for the modification of the Stokes integration kernel or the spectral combination of the different input data (GGM, airborne and terrestrial gravity data, topography gravity signals). Four solutions follow the least squares modification of Stokes's formula with additive corrections (LSMSA) algorithm (Sjöberg 1980, 1981, 1984, 2003). Three solutions performed the data processing using spherical radial basis functions (SRBF), least-squares collocation (LSC) and residual LSC. The variety of parameter choices for the data processing is so large that it is impractical to provide a detailed description of the different computation strategies in this article. We concentrate therefore on the key characteristics considering three main computation stages: handling of topographic effects on gravity (Table 2), prepa-

**Table 2** Methods for estimating the topographic gravity effects within the contributing solutions to the Colorado experiment (FFT – fast Fourier transformation, RTM – residual terrain modeling, DEM – digital elevation model)

Solution	Models	Computation
AUTh	Earth2014, ERTM2160, SRTM 3" v4.1	Gravity anomalies interpolation based on SRTM GBVP solution using spherical harmonics combination Terrestrial data: Earth2014 from degree 720 to 2159 and ERTM2160 from degree 2160 to ~80,000 Airborne data: Earth2014 from degree 720 to 2160
CASM	SRTM 3" v4.1	RTM for airborne and terrestrial data, rectangular prism integration with a 3" DEM and a 5' mean model
CGS	SRTM 3" v4.1	Terrain correction and condensed terrain effect on the geoid with a 3" × 3" DEM within the inner zone (<50 km) The direct topographical effects within the near zone (>50 km and <3°) with a mean 1' DEM; and far-zone (>3°) with a spherical harmonic expansion up to d/o 90 The primary topographical effect within the inner zone (<0.5°) with a mean 30" × 30" DEM; near zone (>0.5 and <2°) with a mean 1' DEM; and far-zone (>2°) with a mean 30' global DEM
Curtin	SRTM 3" v4.1	Terrain correction (for Faye anomalies) based on a binomial expansion up to sixth order using FFT Topographic effects removed in the combination of terrestrial and airborne data based on a rectangular prism integration using a long-wavelength DEM created by spherical harmonic synthesis (maximum degree 300)
DGFI	Earth2014, ERTM2160	Spherical harmonics combination Terrestrial data: Earth2014 from degree 720 to 2159 and ERTM2160 from degree 2160 to ~80,000 Airborne data: Earth2014 from degree 720 to 5480
DTU	SRTM 3" v4.1	RTM for airborne and terrestrial data, rectangular prism integration with a 3" DEM and a 9" mean model. Harmonic correction based on the linear Prey term
Minia	SRTM 3" v4.1	The window topographic–isostatic Airy mass balance principle
GSI	SRTM 3" v4.1, Earth2014	Spherical terrain correction considering the combined effect of topographical and condensation masses based on three DEMs of different resolution: 3" × 3", 1' × 1' and 1° × 1°
IAPG	Earth2014, ERTM2160	Spherical harmonics combination Terrestrial data: Earth2014 from degree 720 to 2159 and ERTM2160 from degree 2160 to ~80,000 Airborne data: Earth2014 from degree 720 to 5400
ITU	SRTM 3" v4.1	RTM for airborne and terrestrial data, rectangular prism integration with a 3" DEM and a 1' mean model
KTH	SRTM 3" v4.1	RTM for airborne and terrestrial data, rectangular prism integration with a 3" DEM and a 5' mean model
NGS	SRTM 3" v4.1	RTM for airborne and terrestrial data, rectangular prism integration with a 3" × 3" DEM and a 1' × 1' mean model
NTIS-GEOF	SRTM 3" v4.1	RTM for airborne and terrestrial data, rectangular prism integration with a 3" DEM for the inner zone (up to 30 km) and 1' for the outer zone (from 30 to 200 km) The mean model is a 5' DEM
Polimi	Same as AUTh	Same as AUTh

ration of surface (terrestrial + airborne) gravity data (Table 3), and solution of the GBVP (Table 4). Table 4 also provides the corresponding bibliographical references describing the detailed computation strategies.

#### 4 Model comparison and validation

All the groups delivered a geoid model on a 1' × 1' grid and geoid heights on the 223 GSVS17 marks; they also provided the geopotential values on the marks and the comparison results can be found in Sánchez et al. (2021). All the groups (except Minia) also provided a quasigeoid model on a 1' × 1' grid and height anomalies on the GSVS17 marks. To simplify the analysis and to focus on the main results, we present in this

**Table 3** Key aspects of the surface (airborne + terrestrial) gravity data preparation within the contributing solutions to the Colorado experiment

Solution	Preprocessing airborne and terrestrial data	Combination of airborne and terrestrial data
AUTh	<p><i>Airborne data:</i>            Molodensky-type free-air anomalies            No filtering            Downward continuation using LSC with planar logarithmic covariance function using residual anomalies (with GGM (XGM2016, d/o = 720) and topographic effects removed)            Covariance function parameters determined from terrestrial data</p> <p><i>Terrestrial data:</i>            Molodensky-type free-air anomalies</p>	<p>Residual anomalies (Molodensky-type anomalies with GGM (XGM2016, d/o = 720) and topographic effects removed)            Unweighted combination of downward continued airborne and terrestrial surface residual anomalies            Gridding: Spline interpolation (tension factor 0.10) to <math>1' \times 1'</math>.  <math>1' \times 1'</math> gridded GGM and topography effects restored</p>
CASM	<p><i>Airborne data:</i>            Gravity disturbances            Filtering with Gaussian filter, length 120 s            Downward continuation implicit in the spectral combination with terrestrial data</p> <p><i>Terrestrial data:</i>            Molodensky-type free-air anomalies</p>	<p>Spectral combination with weights defined according with white and colored noise            Terrestrial data: correlation distance <math>0.5^\circ</math>, weights for white and colored noise: 3.0 mGal and 1.0 mGal, respectively            Airborne gravity: Correlation distance <math>0.5^\circ</math>, weights for white and colored noise: 1.5 mGal, 0.5 mGal, respectively            Gridding: GEOGRID weighted means interpolation to <math>1' \times 1'</math> based on residual gravity disturbances (airborne data) and residual gravity anomalies (terrestrial data). In both cases, GGM (RefB, d/o = 2190) and topography effects removed before interpolation and <math>1' \times 1'</math> gridded GGM and topography effects restored after interpolation</p>
CGS	<p><i>Airborne data:</i>            Observable: gravity disturbances            Filtering: a 3-point smoothing            Downward continuation: inverse Poisson</p> <p><i>Terrestrial data:</i>            Free-air anomalies</p>	<p>Spectral combination of the GGM RefB (up to degree 150 from where it goes into transition with the surface gravity data up to degree 210) and terrestrial gravity data (up to degree 10,800 with a smooth transition at the high-degree end)            Airborne gravity correction for the medium-band (between degrees 210 and 790 with smooth transition backwards at each end), followed by a Gaussian smoothing to the airborne geoid residuals            Mean topographical contribution of <math>1' \times 1'</math> by the primary indirect effect with SRTM v4.1            Gridding: LSC at the mean flight height and Earth's surface</p>
Curtin	<p><i>Airborne data:</i>            Molodensky-type free-air anomalies            Filtering with Gaussian filter, length 80 s            Downward continuation implicit in the LSC used for the combination with terrestrial data</p> <p><i>Terrestrial data:</i>            Molodensky-type free-air anomalies</p>	<p>Residual anomalies (Molodensky-type anomalies with GGM (DIR_R6, d/o = 300) and topography effects removed)            3D LSC with planar logarithmic covariance function            Gridding: LSC interpolation to <math>1' \times 1'</math> included in the airborne and terrestrial data combination  <math>1' \times 1'</math> gridded GGM and topography effects restored</p>
DGFI	<p><i>Airborne data:</i>            Gravity disturbances            Applying a cubic polynomial (CuP) function with smoothing features as a low-pass filter to remove the high-frequency noise in the airborne data after down sampling to 1/8 Hz            Downward continuation implicit in the SRBF approach</p> <p><i>Terrestrial data:</i>            Gravity disturbances</p>	<p>Relative weighting using the method of variance component estimation and regularization parameter determined using the L-curve method            No gridding required</p>
DTU	<p><i>Airborne data:</i>            Molodensky-type free-air anomalies            Filtering with Gaussian filter, length 30 s            Downward continuation implicit in the LSC used for the combination with terrestrial data</p> <p><i>Terrestrial data:</i>            Molodensky-type free-air anomalies</p>	<p>Residual anomalies (Molodensky-type anomalies with GGM (XGM2016, d/o = 300) and topography effects removed)            3D LSC with planar logarithmic covariance function, a-priori error airborne data 2 mGal, a-priori error terrestrial data 1 mGal            Gridding: LSC interpolation to <math>1' \times 1'</math> included in the airborne and terrestrial data combination  <math>1' \times 1'</math> gridded GGM and topography effects restored</p>
Minia	<p><i>Airborne data:</i>            No airborne data used</p> <p><i>Terrestrial data:</i>            Molodensky-type free-air anomalies</p>	<p>Residual anomalies with GGM (RefB, d/o = 2190)            Gridding: Kriging interpolation</p>

Table 3 continued

Solution	Preprocessing airborne and terrestrial data	Combination of airborne and terrestrial data
GSI	<p><i>Airborne data:</i>            Molodensky-type free-air anomalies            Down sampling to 500 m            Downward continuation implicit in the LSC used for the combination with terrestrial data</p> <p><i>Terrestrial data:</i>            Molodensky-type free-air anomalies</p>	Residual anomalies (Molodensky-type anomalies with GGM (XGM2016, $d/o = 719$ ) and topography effects removed) 3D LSC with planar logarithmic covariance function, a-priori error airborne data 2.16 mGal, a-priori error terrestrial data 1.64 mGal Gridding: LSC interpolation to $1' \times 1'$ included in the airborne and terrestrial data combination. $1' \times 1'$ gridded GGM and topography effects restored
IAPG	<p><i>Airborne data:</i>            Gravity disturbances            Filtering with a Gaussian low-pass filter (with a half-width at half-maximum of 3 km), down sampling to 1/32 Hz            Downward continuation implicit in the residual LSC approach</p> <p><i>Terrestrial data:</i>            Gravity disturbances</p>	Relative weighting based on a-priori stochastic modeling No gridding required
ITU	<p><i>Airborne data:</i>            Molodensky-type free-air anomalies            Filtering with Gaussian filter, length 120 s, down sampling to 1 km            Downward continuation implicit in the LSC used for the combination with terrestrial data</p> <p><i>Terrestrial data:</i>            Molodensky-type free-air anomalies</p>	Residual anomalies (Molodensky-type anomalies with GGM (XGM2016, $d/o = 719$ ) and topography effects removed) 3D LSC with planar logarithmic covariance function, a-priori error airborne data 2 mGal, a-priori error terrestrial data 1 mGal Gridding: LSC interpolation to $1' \times 1'$ included in the airborne and terrestrial data combination $1' \times 1'$ gridded GGM and topography effects restored
KTH	<p><i>Airborne data:</i>            Molodensky-type free-air anomalies            Down sampling to <math>3'</math> (<math>\sim 5.5</math> km)            Downward continuation implicit in the LSC used for the combination with terrestrial data</p> <p><i>Terrestrial data:</i>            Molodensky-type free-air anomalies</p>	Residual anomalies (Molodensky-type anomalies with GGM (Ref_B, $n = 2190$ ) and topography effects removed) 3D LSC with spherical covariance function (Tscherning and Rapp, 1974), uncorrelated white noise assumed for both airborne and terrestrial data with standard deviations 2 mGal and 1 mGal, respectively Gridding: LSC interpolation to $0.5' \times 0.5'$ included in the airborne and terrestrial data combination $0.5' \times 0.5'$ gridded GGM and topography effects restored
NGS	<p><i>Airborne data:</i>            Molodensky-type free-air anomalies            Gridded to <math>5' \times 5'</math> and converted to spherical harmonic series, degree 2190            Downward continuation implicit in the spectral combination with terrestrial data</p> <p><i>Terrestrial data:</i>            Molodensky-type free-air anomalies</p>	Spectral combination with weights defined according to white and colored noise Terrestrial data: correlation distance $0.5^\circ$ , weights for white and colored noise: 3.5 mGal and 3.0 mGal, respectively Airborne gravity: Correlation distance $0.25^\circ$ , weights for white and colored noise: 1.5 mGal, 1.0 mGal, respectively Gridding: LSC interpolation to $1' \times 1'$ using refined Bouguer anomalies $1' \times 1'$ gridded Bouguer plate and topography effects restored
NTIS-GEOF	<p><i>Airborne data:</i>            Molodensky-type free-air anomalies            Filtering with Gaussian filter, length 120 s            Downward continuation implicit in the LSC used for the combination with terrestrial data</p> <p><i>Terrestrial data:</i>            Molodensky-type free-air anomalies</p>	Residual anomalies (Molodensky-type anomalies with GGM (XGM2016, $d/o = 500$ ) and topography effects removed) 3D LSC with planar logarithmic covariance function, a-priori error airborne data 3.4 mGal, a-priori error terrestrial data 2.6 mGal Gridding: LSC interpolation to $1' \times 1'$ included in the airborne and terrestrial data combination $1' \times 1'$ gridded GGM and topography effects restored
Polimi	<p><i>Airborne data:</i>            Molodensky-type free-air anomalies            No filtering            Downward continuation using LSC with planar logarithmic covariance function (Forsberg 1987) using residual anomalies (with GGM (XGM2016, <math>d/o = 719</math>) and topographic effects removed). Covariance function parameters determined from terrestrial data</p> <p><i>Terrestrial data:</i>            Molodensky-type free-air anomalies</p>	Residual anomalies (Molodensky-type anomalies with GGM (XGM2016, $d/o = 720$ ) and topography effects removed) Unweighted combination of downward continued airborne and terrestrial surface residual anomalies Gridding: Spline interpolation (tension factor 0.10) to $1' \times 1'$ $1' \times 1'$ gridded GGM and topography effects restored

**Table 4** Key aspects of the geoid and quasigeoid computation within the contributing solutions to the Colorado experiment

Solution	GBVP type and input data	Solution	Results
AUTH	Molodensky scalar-free GGM: XGM2016, $d/o = 719$ Surface data: $1' \times 1'$ Molodensky-type free-air anomalies	RCR, modified Stokes integral (1D FFT) Wong-Gore kernel modification (best-fitting with GPS/leveling), no cap, transition degrees 450 – 719	Height anomaly Converted to geoid using refined Bouguer anomaly Details: Grigoriadis et al. (2021)
CASM	Molodensky scalar-free with terrestrial data Fixed GBVP with airborne data GGM: RefB, $d/o = 2190$ Surface data: $1' \times 1'$ terrestrial Molodensky-type free-air anomalies and $1' \times 1'$ residual airborne gravity disturbances	Spectral combination approach Computation of height anomalies from terrestrial and airborne data independently Spectral combination of the height anomalies of the GGM (up to degree 114 from where it goes into transition with the surface gravity data up to degree 217) and terrestrial and airborne gravity (between degrees 217 and 1,000 with smooth transition at each end) with SRTM model (up to degree 10,800), cap size $1^\circ$	Height anomaly Converted to geoid using refined Bouguer anomalies and the gradient of the gravitational potential Details: Jiang et al. (2020)
CGS	Stokes-Helmert scalar-free GGM: RefB, $d/o = 2190$ Surface data: $1' \times 1'$ airborne and terrestrial Helmert gravity anomalies on the geoid	Modified degree-banded Stokes kernels Modification degree $L = 210$ Cap size $6^\circ$ FFT for numerical integration	Geoid undulation Converted to height anomaly using simple Bouguer anomalies and refined Bouguer anomalies (two results) at the GSVS17 marks Details: Huang and Véronneau (2013)
Curtin	Molodensky scalar-free GGM: RefB, $d/o = 2190$ Surface data: $1' \times 1'$ Faye anomalies (Molodensky-type free-air + terrain correction)	RCR, modified Stokes integral (1D FFT) Wong-Gore kernel modification (best-fitting with GPS/leveling), cap size $0.3^\circ$ , modification degree 360	Height anomaly Converted to geoid using simple Bouguer anomaly Details: Claessens and Filmer (2020)
DGFI	Fixed GBVP GGM: XGM2016, $d/o = 719$ Surface data: Point-wise gravity disturbances	RCR, SRBF The Shannon kernel used for the terrestrial data; and the CuP kernel used for the airborne data The unknown coefficients associated to the kernels determined by the parameter estimation procedure, instead of numerical integration	Height anomaly Converted to geoid using simple Bouguer anomalies Details: Liu et al. (2020)
DTU	Molodensky scalar-free GGM: XGM2016, $d/o = 360$ Surface data: $1' \times 1'$ Molodensky-type free-air anomalies	RCR, modified Stokes integral (spherical FFT) Wong-Gore kernel modification (best-fitting with GPS/leveling data), no cap, transition degrees 180–190, 100% zero padding	Height anomaly Converted to geoid using simple Bouguer anomaly Details: Forsberg and Tscherning (1981), Forsberg (1987), Forsberg and Featherstone (1998)
Minia	Stokes scalar-free GGM: RefB $d/o = 2190$ Surface data: $1' \times 1'$ residual (isostatic) anomalies on the geoid	RCR, modified Stokes integral Meissl (1971) modified kernel, cap size $0.5^\circ$	Geoid undulation No conversion to height anomaly Details: Abd-Elmotaal and Kühtreiber (2003, 2021)
GSI	Stokes scalar-free GGM: XGM2016, $d/o = 719$ Surface data: $1' \times 1'$ residual Helmert gravity anomalies on the geoid	RCR, modified Stokes integral Meissel-Molodensky modified kernel (best-fitting with GPS/leveling), cap size $0.2^\circ$ , modification degree 719	Geoid undulation Converted to height anomaly using simple Bouguer anomalies Details: Matsuo and Forsberg (2021)
IAPG	Fixed GBVP GGM: XGM2018, $d/o = 719$ (very close to XGM2016 but with improved covariance information) Surface data: Point-wise gravity disturbances	RCR, residual LSC Statistical least-squares optimization Covariance matrices for all input quantities (GGM, topographic reduction, observation accuracy) to result in a realistic modeling of the gravity field and the error budget	Height anomaly Converted to geoid using simple Bouguer anomalies Details: Willberg et al. (2019, 2020)



**Table 4** continued

Solution	GBVP type and input data	Solution	Results
ITU	Molodensky scalar-free-GGM: XGM2016, d/o = 719 Surface data: 1' × 1' Molodensky-type free-air anomalies	LSMSA Kernel modification based on unbiased solution of least squares modification parameters, standard deviation of surface gravity anomalies 3 mGal, cap size 0.5°, kernel modification degree equal to maximum GGM coefficient (degree 719)	Height anomaly Converted to geoid using simple Bouguer anomalies Details: Işık et al. (2021)
KTH	Molodensky scalar-free-GGM: GOCO05S, d/o = 240 Surface data: 0.5' × 0.5' Molodensky-type free-air anomalies	LSMSA Least-squares modification with satellite-only GGM Signal degree variances according to Tscherning and Rapp (1974) Error degree variances as a combination of white noise (σ = 1 mGal) and colored noise (σ = 0.5 mGal with correlation-length 0.5 degrees), cap size 2°	Height anomaly Converted to geoid using simple Bouguer anomalies Details: Ågren et al. (2009)
NGS	Molodensky scalar-free-GGM: RefB, d/o = 2190 Surface data: 1' × 1' Molodensky-type free-air anomalies	RCR, modified Stokes integral Wong-Gore kernel modification (best-fitting with GPS/leveling data), cap size 1°, modification degree 980	Height anomaly Converted to geoid using simple Bouguer anomalies Details: Wang et al. (2020)
NTIS-GEOF	Molodensky scalar-free-GGM: XGM2016, d/o = 500 Surface data: 1' × 1' Molodensky-type free-air anomalies	LSMSA Kernel modification based on a biased solution of least squares modification parameters, cap size 0.5°	Geoid undulation Converted to height anomaly using refined Bouguer anomalies- Details: Varga et al. (2021)
Polimi	Molodensky scalar-free-GGM: XGM2016, d/o = 719 Surface data: 1' × 1' Molodensky-type free-air anomalies	RCR, LSC Signal variances according to the spherical covariance function of Tscherning and Rapp (1974)	Height anomaly Converted to geoid using refined Bouguer anomalies Details: Grigoriadis et al. (2021)

paper the comparison between the quasigeoid models only; the comparison between the geoid models produces very similar results and conclusions. As mentioned, 11 groups delivered quasigeoid models as their primary solutions, while three groups computed the geoid models directly (cf. Table 4). These three geoid models were converted into quasigeoid models by applying exactly the same geoid-quasigeoid conversion term (see Sect. 4.1). In this way, we avoid possible sources of discrepancy caused by the different conversion terms used in the *converted* models (cf. Table 4) and expect that the discrepancies between the results are mainly caused by the different data processing and GBVP solution strategies.

### 4.1 Geoid-quasigeoid separation term

The simple geoid-quasigeoid separation (GQS) uses the Bouguer anomaly  $\Delta g_B$  (Heiskanen and Moritz 1967, Sect. 8–13) to approximate the difference between the mean *real* gravity and mean normal gravity:

$$N - \zeta = \frac{\Delta g_B(P)}{\bar{\gamma}} H, \tag{1}$$

where  $\bar{\gamma}$  is the mean normal gravity (GRS80) along the normal plumb line,  $H$  is the orthometric height,  $N$  and  $\zeta$  are the geoid undulation and the height anomaly, respectively.

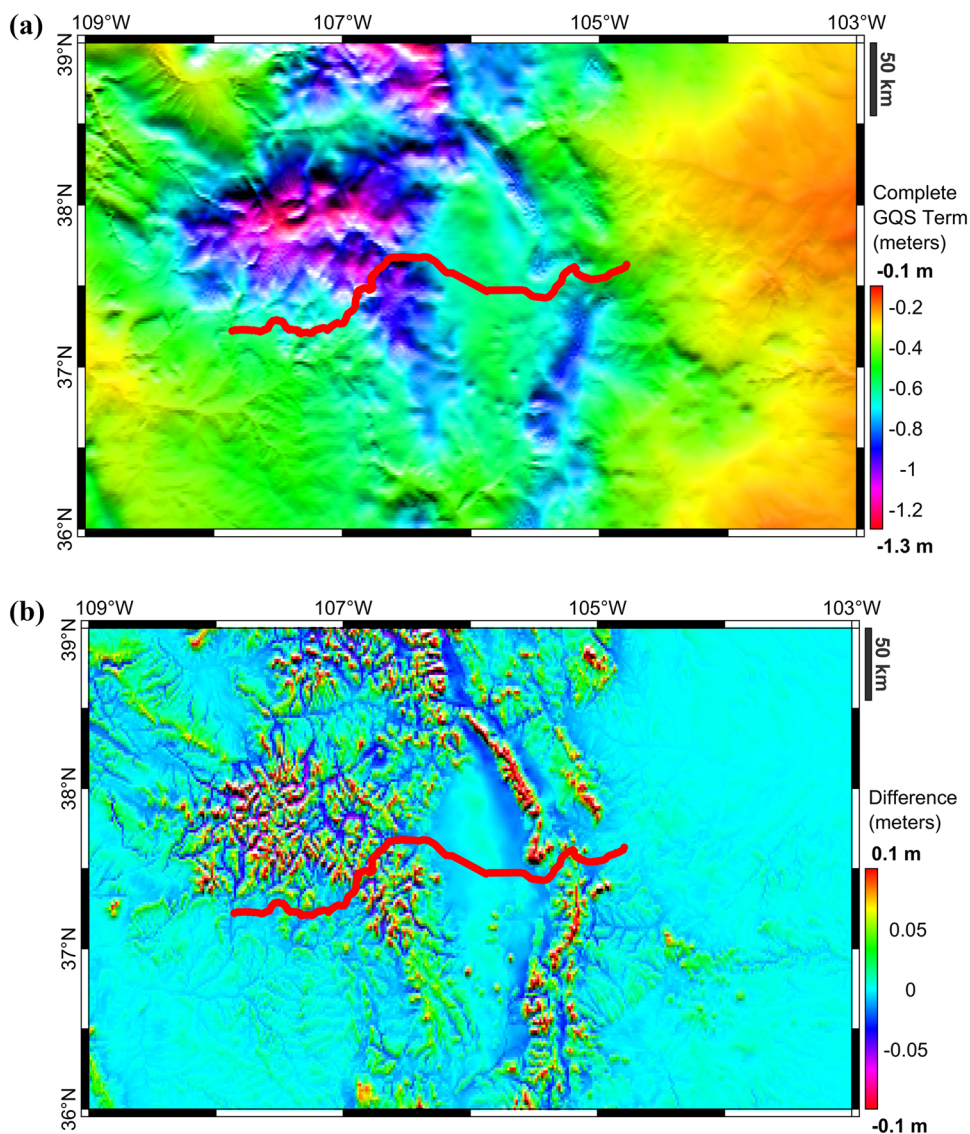
More accurate formulations were developed by, e.g., Flury and Rummel (2009) and Sjöberg (2010). In this paper, the separation GQS is computed in terms of the Bouguer disturbance  $\delta g_B$  using Wang et al. (2021):

$$N - \zeta = \frac{\delta g_B(P)}{\bar{\gamma}} H + \frac{V_t(Q) - V_t(P)}{\bar{\gamma}} - \frac{H^2}{2\bar{\gamma}} \frac{\partial \delta g_B}{\partial H}, \tag{2}$$

where the second and third terms in Eq. (2) are known as the potential and gravity gradient corrections, respectively.  $V_t$  is the gravitational potential of the topographic masses.  $P$  is located on the Earth's surface and  $Q$  is the projection (along the plumb line) of  $P$  on the geoid. To distinguish the simple GQS in Eq. (1) from the separation defined in Eq. (2), the latter is called the complete separation term hereafter.

The computation of the Bouguer disturbance and the topographic potential at the points  $P$  and  $Q$  requires global integrations. Because of the canceling effect between  $V_t(P)$  and  $V_t(Q)$ , and taking into consideration the high frequencies contained in the corrections, the integration radius was

**Fig. 3** **a** Complete GQS term (Eq. (2)), unit in meter. Mean = -0.454, Min = -1.257, Max = -0.127, STD = 0.223, RMS = 0.506. **b** Differences between the complete and simple GQS term (Eq. (2) – Eq. (1)), unit in meter. Mean = -0.005, Min = -0.094, Max = 0.277, STD = 0.021, RMS = 0.021



limited to a one-degree cap. The complete GQS was computed for the experimental geoid 2020 (Wang et al., 2021) and the Colorado area is a part of it. Figure 3a, b show the GQS term computed using Eq. (2) and the differences computed using Eqs. (1) and (2), respectively. The differences reach 27.7 cm in the extreme case, and 2.1 cm in terms of root mean square (RMS) values (see Fig. 3b).

The improvement offered by Eq. (2) is implied by the fact that the CGS model (under the Helmert-Stokes scheme) gets closer to NGS model (under the Molodensky theory) when the complete separation term is used. The STD of the differences between these two models is reduced from 3.1 cm to 2.2 cm. For this reason, the complete separation is applied to the three geoid models (CGS, Minia and GSI) in the following analysis.

#### 4.2 Quasigeoid area comparisons (grids of $1' \times 1'$ )

The models provided by the contributing groups are given on a  $1' \times 1'$  grid over the study area between latitudes 36° N to 39° N and longitudes 109° W to 103° W. This study area has been reduced by a one-degree border along each side with respect to the area covered by the gravity data (Fig. 1) to reduce edge effects in the quasigeoid models. As the grids are submitted in different formats (point values and lines of scan) and in different cell registrations (center and corner), the first step was to transform the grids to a common format, and then to interpolate the quasigeoid models onto  $1' \times 1'$  grids with a common registration (hereafter called standardized grids). To show the precision of the models, the 14 quasigeoid models were compared with the group mean. In the end, the height anomalies were interpolated on the GSVS17 marks from the

**Table 5** Statistics of the differences among the individual quasigeoid models and the mean of all quasigeoid models at the  $1' \times 1'$  grid; 85 cm was added to Minia model. Units in cm

	Mean	STD	RMS	Min	Max	Range
AUTh	0.4	1.8	1.9	-11.2	6.3	17.5
CASM	0.5	1.9	1.9	-12.0	17.1	29.1
CGS	-0.4	2.0	2.0	-10.8	14.7	25.5
Curtin	0.3	2.3	2.3	-17.8	10.1	27.9
DGFI	-0.6	1.5	1.6	-9.1	7.0	16.1
DTU	1.1	2.8	3.1	-18.1	18.2	36.3
Minia	0.5	5.1	5.1	-12.9	17.7	30.6
GSI	-0.7	2.9	3.0	-29.4	17.9	47.3
IAPG	-1.1	1.8	2.1	-13.8	6.5	20.3
ITU	0.5	5.3	5.3	-45.2	22.9	68.1
KTH	-0.3	1.7	1.8	-11.6	8.8	20.4
NGS	0.0	1.9	1.9	-7.9	13.9	21.8
NTIS-GEOF	-1.6	2.7	3.2	-19.6	13.2	32.8
Polimi	1.2	1.8	2.2	-6.5	14.8	21.3

14 standardized (quasi)geoid grids and compared, without using the values provided by the research groups.

Figure 4 illustrates the mean height anomalies obtained from the 14 standardized grids. An 85 cm bias had to be added to the Minia model as its zero-degree geoid term is related to the historical GPS/leveling data set (see Sect. 2) and it reflects the bias of the NAVD88 datum with respect to the global vertical datum introduced by the IHRF  $W_0$  value (see more details in Sect. 4.3).

To highlight the agreement (or disagreement) among the models, the statistics of the model differences to the mean of all quasigeoid models are listed in Table 5.

The RMS values of the individual solutions vary between 1.6 and 5.3 cm and have a median of 2.0 cm. From this comparison, we suggest that  $\sim 2$  cm can be considered a reasonable approximation for the precision of the 14 quasigeoid models. This is a significant result in this rugged mountainous area after two guided iterations, and a good accuracy indication of current quasigeoid computations. However, the precision does not meet the 1-cm target, demonstrating the need for further research, including the capability to be able to accurately validate sub-cm quasigeoid models. Table 5 also indicates large variations in the differences among the ranges, with extreme cases of more than 40 cm. Indeed, the median value of the difference among ranges is 26.7 cm, which is also quite large.

To visualize the spatial distribution of the discrepancies between the models, the standard deviation values of the height anomaly differences (14 samples) in each  $1' \times 1'$  cell were computed and are shown in Fig. 5. Large differences are strongly correlated with the roughness and height of the

topography, and in areas where terrestrial gravity data are missing or sparse (see Fig. 1).

### 4.3 GSVS17 GPS/leveling comparisons

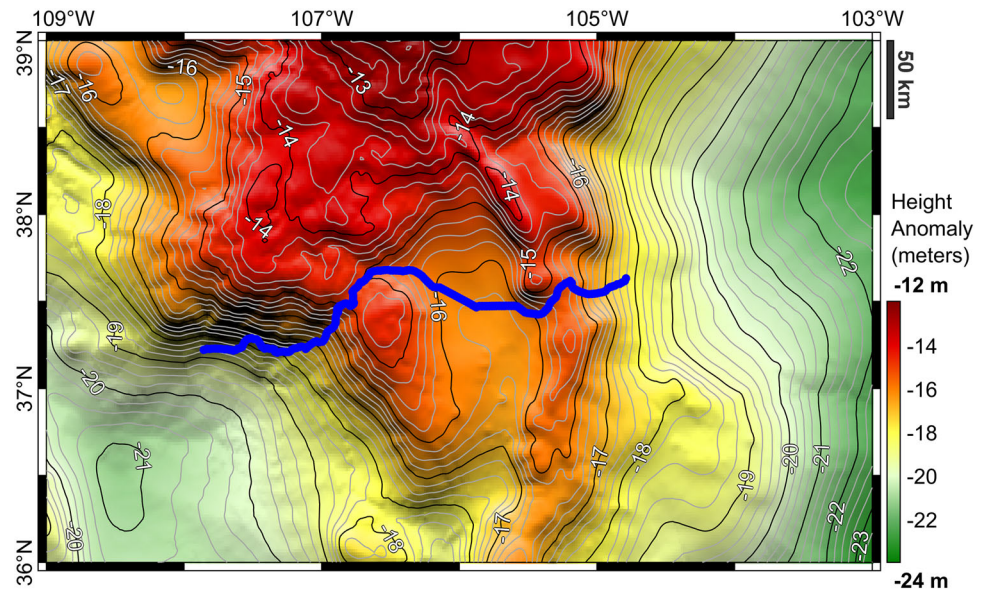
The GSVS17 geopotential numbers are adjusted by holding the mark (ID 223) in Walsenburg fixed with the height of 1908.624 m (NAVD88) multiplied by the observed gravity value at this point to get a reference potential value. The normal heights  $H^N$  are computed using the adjusted GSVS17 geopotential numbers and GRS80 normal gravity values. Afterward, the GSVS17 height anomalies  $\zeta_{GSVS17}$  are obtained by removing the normal height  $H^N$  from the ellipsoidal height  $h_{GPS}$  on the 223 marks ( $\zeta_{GSVS17} = h_{GPS} - H^N$ ). Note that the GSVS17 data were not available to any of the contributing groups, so that the GSVS17 data could not be used to tune quasigeoid models, but were used solely for an independent comparison.

Figure 6 illustrates the differences between the height anomalies estimated by the contributing groups and the GSVS17-derived height anomalies.

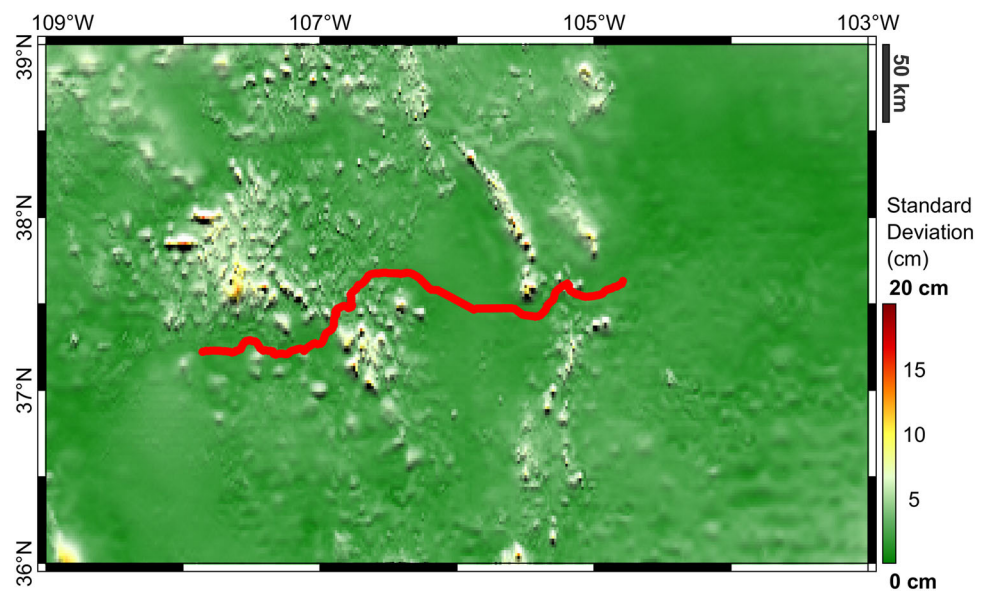
Figure 6 shows the 88 cm bias (cf. Table 6) between the models and the GSVS17 height anomalies. This bias can be explained primarily as the  $W_0$  value adopted for this experiment differs from that defined by the NAVD88 datum, which is tied to the tide gauge at Rimouski (Zilkoski et al. 1992), and secondly, by errors in the NAVD88 data (GPS and leveling data). Excluding the bias, the profiles in Fig. 6 show no apparent tilt from mark 1 to mark 160 (about 250 km distance) and the differences are limited to a narrow range. A noticeable minimum after mark 160 is seen. All quasigeoid models behave similarly. At this point, we do not know the causes of the minimum. More studies are needed to determine whether it is caused by errors in the GSVS17 data or in the gravity data, or in both. The statistics of the height anomaly differences between the quasigeoid models and GSVS17 are given in Table 6.

After removing the mean values, the quasigeoid models agree with the GSVS17 height anomalies in the range from 1.7 to 3.6 cm in terms of the STD at the 223 marks. The median of the STD values is 3.1 cm. The CGS model agrees most closely with the GSVS17 data with a STD value of 1.7 cm. If the errors in the GSVS17 GPS/leveling data and in the quasigeoid models are uncorrelated (most likely), then the STD of 1.7 cm cautiously suggests that the accuracy of the GSVS17 height anomalies is not worse than this value. Of course, it is always possible that some errors in the gravimetric quasigeoid and the GPS/leveling data are the same and canceled out. Because this is an independent test using the GSVS17 data, we assume in the following analysis that the errors in both the GSVS17-derived height anomalies and the gravimetric height anomalies from the quasigeoid models are also independent.

**Fig. 4** The mean quasigeoid model at the  $1' \times 1'$  grid computed from the 14 quasigeoid models. The blue line represents the GSVS17 profile along the highway US 160 from Durango to Walsenburg



**Fig. 5** Standard deviation (STD) values of the height anomalies from all models at a  $1' \times 1'$  grid, unit in cm. The STD values have the area mean of 2.7 cm and range from 0.6 to 13.1 cm. The red line represents the GSVS17 profile along the highway US 160 from Durango to Walsenburg. It does not pass the roughest terrain in the region



Based on the preliminary analysis of the GSVS17 data, especially the height anomalies computed from the deflections of the vertical (Ahlgren, personal communication, 2021), we estimate the accuracy of the GSVS17-derived height anomalies is about 1.2 cm. Consequently, accuracies of the gravimetric quasigeoid models are estimated between 1.2 and 3.4 cm. The mean quasigeoid model is also evaluated using the GSVS17-based height anomalies and agrees better than most of the individual models. Its accuracy is estimated as 2.3 cm.

To demonstrate more clearly the agreement between the gravimetric models and the GSVS17 data, the height anomaly differences of the CGS and the mean models are plotted in Fig. 7.

Figure 7 shows that the mean model has similar smaller features as the CGS model before the mark 160, and the mean model is 1.4 cm higher than the CGS model. The offset is consistent with the 1.1 cm standard deviation of the mean residuals shown in Table 6, which characterize the uncertainty due to methodology. Both sets of height anomalies decrease after mark 160, and the CGS model decreases less: the differences of the mean model have a 10-cm slope relative to the GSVS17 data from mark 160 to 193, whereas the slope of the CGS model is 5 cm. The smaller slope of the CGS model after the mark 160 is reflected in the smaller STD of the differences (1.7 cm) than the STD values of the mean model (2.6 cm). Another notable feature is that both models agree well at the first peak of height 3310 m (mark

**Fig. 6** Residual height anomalies along the GSVS17 traverse ( $\zeta_{\text{model}} - \zeta_{\text{GSVS17}}$ ). 85 cm was added to the Minia solution

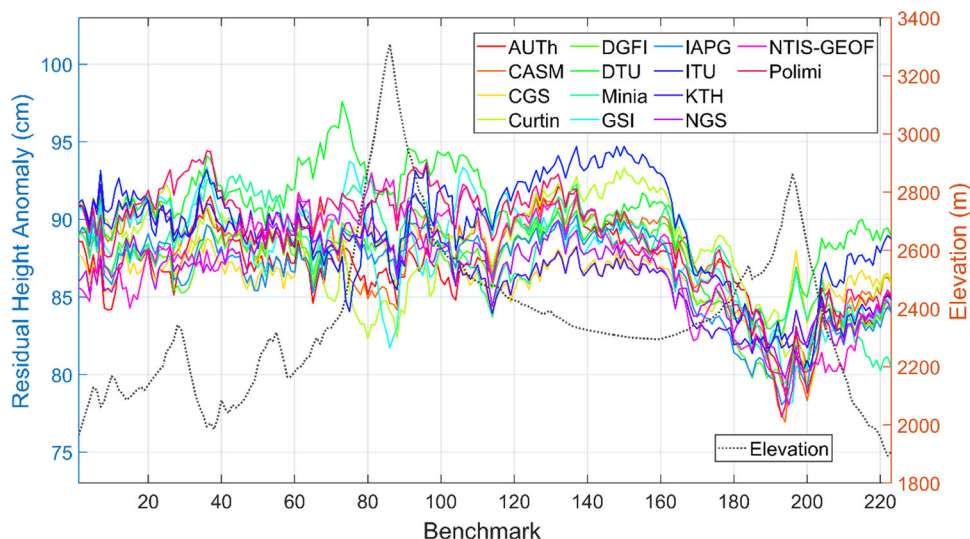


**Table 6** Statistics of the differences between the height anomalies provided by the individual solutions and the height anomalies inferred from the leveling-based geopotential numbers and GPS positioning along the GSVS17 profile ( $\zeta_{\text{model}} - \zeta_{\text{GSVS17}}$ ), units in cm

	Mean	STD	RMS	Min	Max	Range
AUTh	86.9	2.5	87.0	78.9	92.1	13.2
CASM	87.6	3.1	87.7	76.9	91.5	14.6
CGS	86.5	<i>1.7</i>	<i>86.5</i>	<i>81.5</i>	<i>90.1</i>	<i>8.6</i>
Curtin	88.0	3.2	88.0	79.1	93.3	14.2
DGFI	87.0	2.9	87.1	79.4	91.5	12.1
DTU	90.2	3.0	90.2	82.9	97.6	14.6
<i>Minia</i>	<i>7.0</i>	<i>3.1</i>	<i>7.6</i>	<i>0.7</i>	<i>11.9</i>	<i>12.6</i>
<i>GSI</i>	<i>87.8</i>	<i>3.2</i>	<i>87.9</i>	<i>78.2</i>	<i>93.7</i>	<i>15.6</i>
IAPG	86.5	2.9	86.6	78.1	90.3	12.2
ITU	89.4	3.4	89.4	80.3	94.7	14.4
KTH	87.0	2.8	87.0	81.4	92.2	10.9
NGS	86.6	2.3	86.7	79.7	91.3	11.6
NTIS-GEOF	87.2	3.5	87.3	78.0	93.0	15.0
Polimi	88.9	3.6	88.9	77.3	94.4	17.1
Mean*	87.9	2.6	88.0	80.4	91.3	10.9

\*Mean value excludes the Minia model. Values of three converted models (CGS, Minia and GSI) are in italics

86), where the elevation raises from 2200 to 3300 m in about 60 km distance.

#### 4.4 GSVS17 differential quasigeoid (slope) comparisons

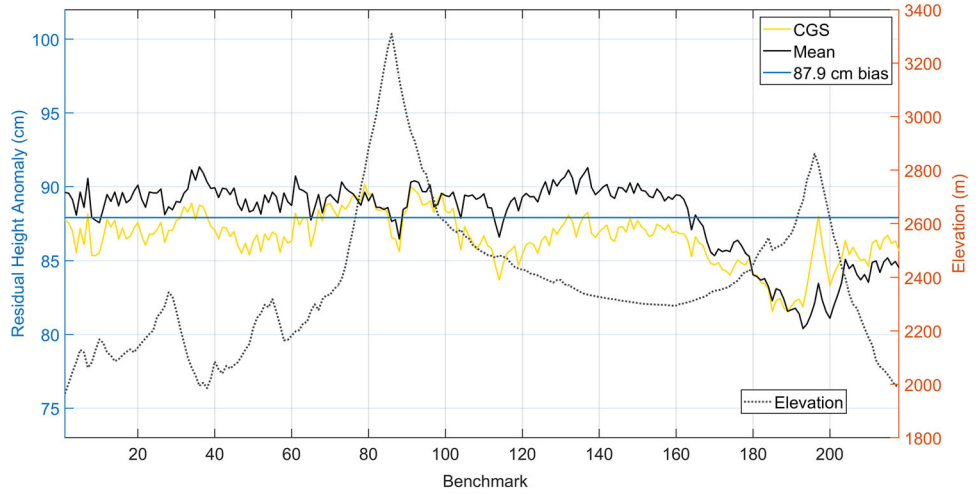
Similar to the GSVS comparisons (Smith et al. 2013; Wang et al. 2017b; van Westrum et al. 2021), and to assess the relative accuracy of the quasigeoid models, a differential quasigeoid comparison is performed for all the contributing solutions. In the same way as described in Smith et al.

(2013), the 24,531 pairs were grouped into 12 bins, containing approximately 2,000 pairs each. Then, the RMS values of height anomaly differences were computed for the 12 bins. The results are illustrated in Fig. 8. The five models in the best agreement are highlighted. The RMS values range from 2 to 3 cm for these five models at baseline lengths from 2 to 100 km, and then, they disagree up to 6 cm at longer baseline lengths. The CGS model presents RMS values between 2 and 3 cm in every baseline length.

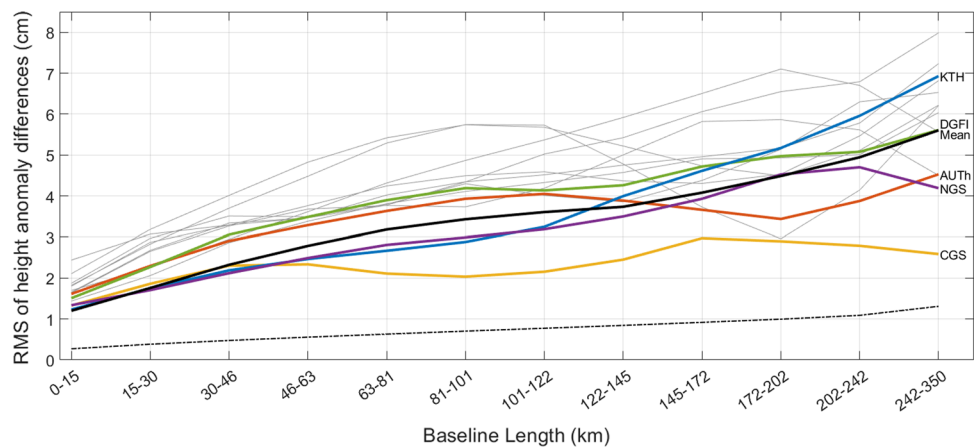
The RMS values of the differences for the remaining models vary from 2 to 8 cm for different baseline lengths. The RMS values increase with respect to the baseline length, which resembles the trend of propagated leveling error. The dotted line is the formal error of the GSVS17 leveled heights based on the empirical formula  $0.7\sqrt{d}$  mm (Zilkoski et al. 1992), where  $d$  is the distance between two marks in km. The formal error reaches its maximum at 1.6 cm at the distance of 350 km and cannot explain the larger RMS values in Fig. 8. To identify the error sources, the RMS differences were computed only for the portion of the line between marks 1 and 160 and plotted in Fig. 9.

Figure 9 shows the RMS differences of quasigeoid slopes from mark 1 to 160. In comparison with Fig. 8, the systematic trend disappears for most of the models. The large differences after mark 160 (see Fig. 6) are the major contributor to the large RMS differences and the systematic trend in Fig. 8. It is also interesting to see that the mean model agrees with the GSVS17 data the best at every baseline length, likely due to its averaging effect to the random errors in all the individual models. Since the RMS differences contain the errors of the quasigeoid models and the GPS/leveling, the formal leveling error should not be larger than that. The formal error of the leveled height in Fig. 9 indicates that the formal error is properly assigned. Another observation from Fig. 9 is that the mean model reaches 1-cm (relative) accuracy in this best

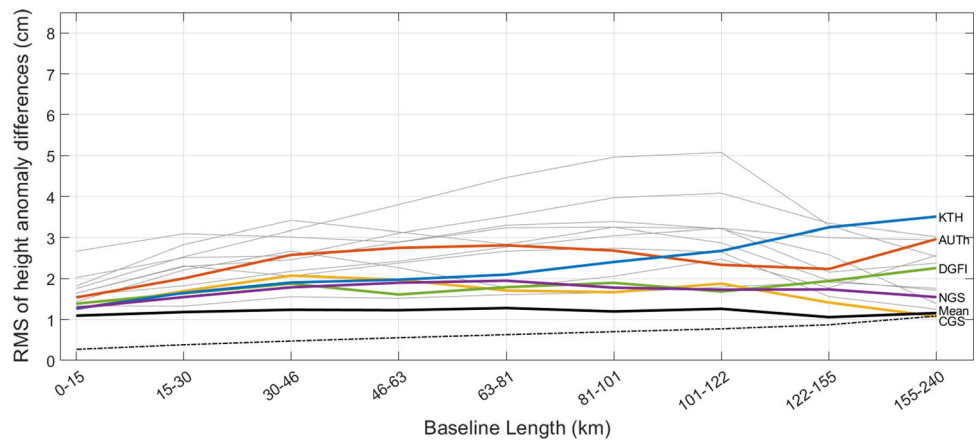
**Fig. 7** Differences between the CGS, the mean of all quasigeoid models and the GSVS17-derived heights anomalies ( $\zeta_{\text{model}} - \zeta_{\text{GSVS17}}$ )



**Fig. 8** Quasigeoid slope comparisons. Colored lines highlight the five best agreement models. Black line represents the mean value based on the 14 individual solutions. The formal error of the leveled height is shown as the dotted line. Highlighted models are the following: Mean = black, AUTH = red, CGS = yellow, DGFI = green, KTH = blue, NGS = purple



**Fig. 9** Quasigeoid slope comparisons between marks 1 and 160 (baseline length 250 km). The formal error of the leveled height is shown as the dotted line. Highlighted models are the following: Mean = black, AUTH = red, CGS = yellow, DGFI = green, KTH = blue, NGS = purple



scenario (mark 1 to 160), but the precision of the individual models still needs to be improved further.

The RMS values obtained in the quasigeoid slope comparison of the individual models with the GSVS17 data at different baseline lengths are listed in Table 7. The differential comparisons of the geoid slope provide very similar results as the height anomaly slope comparisons and so are not included here.

### 5 Discussion and conclusions

Fourteen groups from thirteen countries participated in the Colorado 1-cm geoid experiment. The member groups computed geoid heights, height anomalies and geopotential values at the 223 GSVS17 marks. In addition, the groups submitted 14 geoid models and 13 quasigeoid models at 1' x 1' grids covering the Colorado area. This paper evaluates the

**Table 7** RMS values obtained in the quasi-geoid slope comparisons at different baseline lengths, number of pairs is the count of height anomaly differences at a particular baseline length. Unit in cm

ID	Baseline length in km // number of pairs													
	0-15 // 2038	15-30 // 2034	30-46 // 2067	46-63 // 2070	63-81 // 2068	81-101 // 2153	101-122 // 2063	122-145 // 1984	145-172 // 2057	172-202 // 1975	202-242 // 2012	242-350 // 2010		
AUTH	1.6	2.3	2.9	3.3	3.6	3.9	4.0	3.9	3.7	3.4	3.9	4.5		
CASM	1.8	2.9	3.3	3.8	4.2	4.5	4.6	4.4	4.3	4.5	5.5	6.8		
CGS	1.3	1.9	2.3	2.3	2.1	2.0	2.2	2.5	3.0	2.9	2.8	2.6		
Curtin	1.8	2.8	3.7	4.5	5.3	5.7	5.7	4.8	3.7	3.0	4.1	6.2		
DGFI	1.5	2.3	3.1	3.5	3.9	4.2	4.1	4.3	4.7	5.0	5.1	5.6		
DTU	1.6	2.7	3.3	3.7	3.8	3.7	4.2	5.0	5.8	5.9	5.6	4.5		
Mimia	1.9	3.0	3.5	3.5	3.8	4.3	4.0	3.9	4.4	5.1	6.3	6.5		
GSI	2.4	3.1	3.3	3.5	4.0	4.3	4.5	4.8	5.0	5.2	5.8	7.2		
IAPG	1.4	2.1	2.9	3.4	3.8	4.1	4.3	4.6	4.9	4.9	5.0	6.0		
ITU	2.1	3.2	4.0	4.8	5.4	5.7	5.7	5.2	4.7	4.5	5.1	6.2		
KTH	1.2	1.8	2.2	2.5	2.7	2.9	3.2	4.0	4.6	5.2	6.0	6.9		
NGS	1.3	1.7	2.1	2.5	2.8	3.0	3.2	3.5	3.9	4.5	4.7	4.2		
NTIS-GEOF	1.7	2.2	2.9	3.6	4.3	4.9	5.4	5.9	6.5	7.1	6.7	5.6		
Polimi	1.7	2.7	3.3	3.5	3.8	4.3	5.0	5.4	6.1	6.5	6.8	8.0		
Mean	1.2	1.8	2.3	2.8	3.2	3.4	3.6	3.7	4.1	4.5	4.9	5.6		

results in terms of height anomalies by comparing the quasi-geoid models in three different ways: a) comparison of the  $1' \times 1'$  grids to assess the model precision, b) comparison with the GSVS17 data to estimate the model accuracy (relative), and c) a slope comparison to evaluate the agreement between the GSVS17 height anomalies and the gravimetric quasigeoid models at different baseline lengths.

The grid comparison suggests that the precision of the models is  $\sim 2.0$  cm. This is an important achievement considering the large topographic gradients existing in Colorado. However, this precision does not reach the target value of 1 cm. Further steps are needed to identify the causes of the differences and to improve the precision of the computation methods, or methodologic differences below 1 cm.

Most models agree with the GSVS17 height anomalies to  $\sim 2$  cm before mark 160, after which the models behave similarly with each other, but differ from the leveling by 5 to 10 cm. The CGS model behaves similarly, but agrees with GSVS17 better than the rest of the models after that mark. This is reflected by the smallest STD of the height anomaly differences (1.7 cm). The STD of other models range from 2.1 cm to 3.6 cm. The median of the STD is 3.1 cm. Under the no-correlation assumption between the errors in gravimetric quasigeoid models and the GSVS17 GPS/leveling data, and using 1.2 cm accuracy of the GSVS17 heights anomalies, the CGS quasigeoid model is estimated to have 1.2 cm accuracy on those GSVS17 marks. Because the GSVS17 traverse does not pass the roughest terrain in the region, a 2 cm accuracy for the quasigeoid model that best agrees with GSVS17 could be a reasonable assessment for this experiment. The GSVS17 comparisons indicate that the 1-cm geoid may be possible even in rugged mountains if accurate and well distributed gravity data, as well as detailed DEMs are available, as Figs. 7 and 9 suggested for the segment before mark 160.

The differential (slope) quasigeoid comparisons show the RMS differences increase with respect to the baseline length generally (Fig. 8). The RMS values range from 2 to 3 cm for the five highlighted models at baseline lengths from 2 to 100 km, and then they disagree up to 8 cm at longer baseline lengths. The larger RMS differences and the systematic trend in Fig. 8 are caused mostly by the large differences after mark 160.

The Colorado experiment has indicated that quasigeoid models can be computed to 2 cm precision, and that the accuracy may reach 2 cm in the region. A caveat here is the assumption that the GSVS17 used as the test data is independent and has an accuracy of 1.2 cm. The small difference (STD 1.7 cm) between the CGS model and GSVS17-derived height anomalies tends to support this accuracy assessment, noting that providing test data with sub-cm accuracy to verify that 1-cm geoid accuracy has been achieved may be as challenging as achieving the 1 cm geoid itself.

At this point, even if the model under the Helmert-Stokes scheme agrees with the GSVS17 data the best, it is not sufficient to claim its superiority over other methods. A consensus is that the theoretical approaches should be equivalent and up to the same accuracy, so that the differences occur in the numerical computations and the data processing techniques. Differences in data editing, interpolation, data combination and gridding all contribute to differences, as do differences in use of the reference gravity models (kernel modification/truncation), and different ways to combine terrestrial and airborne gravity data. These issues need to be investigated further for their effects on the differences.

It needs to be pointed out that the models computed for the experiment are under the constant density assumption. This assumption affects the geoid computation directly, but it would not affect the computation of the quasigeoid if the gravity data were given everywhere. In practice, the topography has been used to aid the interpolation of gravity data into a regular grid (e.g., use of the Bouguer gravity anomaly or RTM gravity), and thus the constant density assumption is not completely exempt from the quasigeoid computation. Whether its effect is negligible needs to be assessed in future studies to ensure the 1-cm geoid accuracy.

The Colorado experiment is an effort by the international geodetic community coordinated by IAG to examine (quasi)geoid disagreements caused by computation methods and software used by different groups. In addition, the experiment tries to assess the accuracy of the computed (quasi)geoid models and geopotential values (Sánchez et al. 2021) by using the newly collected GSVS17 data in Colorado. Because of the relative sense of leveling data, the accuracy assessment in this paper is considered as relative.

It is challenging to explain fully the differences among the (quasi)geoid models for this experiment due to specific data processing techniques, computational procedures, and combination schemes. To achieve 1-cm geoid computations among all the methods, a series of recommendations has been set out that will be used to guide further collaborative experiments:

- Examine topographical reductions, data interpolation, and downward continuation steps. For example, RTM-based free-air anomalies vs TC-based Bouguer anomalies for interpolation
- Tune the spectral and LSC combinations of global model, airborne and terrestrial gravity data. For instance, adjust weights and error variances optimally
- Select a common reference model, a proper radius of numerical integration, and optimal kernel modification parameters
- Study and understand biases among the models, especially between LSC solutions and others among other causes



- Compare various (quasi)geoid models computed by different international teams
- Improve agreement with the released GSVS17 GPS/leveling and deflections of the vertical data, which are the best independent validation datasets available
- Further evaluation of GSVS17 and other high accuracy test sites with sub-cm accuracies to ensure the 1-cm geoid can be verified when it is achieved

**Acknowledgements** This study was possible thanks to a strong international cooperation coordinated within IAG, in particular, the IAG Sub-commission 2.2: Methodology for geoid and physical height systems (Ågren and Ellmann 2019); the joint working group 2.2.2: The 1-cm geoid experiment in Colorado (Wang and Forsberg, 2019); the study group 0.15: Regional geoid/quasigeoid modeling—Theoretical framework for the sub-centimeter accuracy of the IAG Inter-Commission Committee on Theory – ICCT (Huang and Wang 2019); and the working group 0.1.2: Strategy for the realization of the IHRS of the Focus Area Unified Height System of the Global Geodetic Observing System—G-GOS (Sánchez, 2019; Sánchez and Barzaghi 2020). The authors are especially indebted to the National Geodetic Survey for providing the gravity, topographic and GPS/leveling data sets for this experiment. The authors thank three anonymous reviewers, the Associate Editor and Editor for their time, constructive suggestions and comments, which helped improving the initial version of this manuscript.

**Author contributions** YMW, LS, JÅ, JH and RF conceptualized and coordinated the Colorado experiment, outlined the standards for the data processing, participated in the computation of the solutions NGS, DGFI, KTH, CGS and DTU and prepared the original draft. YMW, XL, KA and JK computed the solution NGS and performed the comparison/evaluation of the delivered solutions. VNG, GSV and DAN computed the solution AUTH. TJ computed the solution CASM. MVé and JH computed the solution CGS. SC and MF computed the solution Curtin. QL, MS and LS computed the solution DGFI. RF computed the solution DTU. HAAE computed the solution Minia. KM computed the solution GSI. MW, PZ and RP computed the solution IAPG. BE, MSI and SE computed the solution ITU. JÅ computed the solution KTH .

MV, TB, MP and PN computed the solution NTIS-GEOF. RB, DC and ÖK computed the solution Polimi. All authors contributed to review and editing.

**Data availability** The data that support the findings of this study are publically available here: <https://geodesy.noaa.gov/GEOID/research/co-cm-experiment/>; <https://geodesy.noaa.gov/GEOID/GSVS17/index.shtml>; The airborne gravity data are available at NGS: [https://www.ngs.noaa.gov/GRAV-D/data\\_ms05.shtml](https://www.ngs.noaa.gov/GRAV-D/data_ms05.shtml); The standardized 1' × 1' geoid, quasigeoid grids, input and validation data sets are available at the International Service for the Geoid (Reguzzoni et al. 2021) [https://www.isgeoid.polimi.it/Projects/colorado\\_experiment.html](https://www.isgeoid.polimi.it/Projects/colorado_experiment.html)

## Appendix. Fundamental parameters, zero-degree harmonic treatment and computation requirements

Fundamental parameters, zero-degree harmonic treatment and computation requirements.

Since a main objective of the Colorado experiment is to compare gravity functionals (i.e., geoid, quasigeoid, potential values) determined using different methodologies, it was necessary to outline a set of basic (minimum) requirements to standardize as much as possible the data processing to avoid gross discrepancies as those caused for instance using different reference ellipsoids or permanent-tide systems. In this way, in addition to the use of the same input data (described in Sect. 3), we agreed to follow the conventions summarized in Table 8.

**Table 8** Constants and conventions agreed within the Colorado experiment (cf. Sánchez et al. 2018)

Constant/convention	Comment
<i>General constants</i>	
$G$ : $6.674\ 28 \times 10^{-11}\ \text{m}^3\ \text{kg}^{-1}\ \text{s}^{-2}$	Universal gravitational constant
$GM_{\text{GGM}}$ : $3.986\ 004\ 415 \times 10^{14}\ \text{m}^3\ \text{s}^{-2}$	Geocentric gravitational constant, including the mass of the Earth's atmosphere (Ries et al. 1992)
$W_0$ : $62\ 636\ 853.4\ \text{m}^2\ \text{s}^{-2}$	Conventional reference potential value of the geoid (IHR reference value adopted by the IAG Resolution No. 1 (2015), Drewes et al. 2016, p. 981)
$\rho$ : $2670\ \text{kg}\ \text{m}^{-3}$	Average density of topographic masses (for geoid computation)
<i>Reference ellipsoid</i>	
Geodetic Reference System 1980 (GRS80)	Standard for computation of gravity anomalies, gravity disturbances, disturbing potential, geodetic coordinates, geoid heights, height anomalies, etc. All parameters are specified in Moritz (2000)
<i>Permanent tide</i>	
Tide-free (non-tide) system	According to the IAG Resolution No. 16 (1983) (Tscherning, 1984), the zero-tide system is to be used for the Earth's gravity field and crust modeling. According to the IAG Resolution No. 1 (2015), the mean system should be used for the final potential values. However, we decide to use the tide-free system in the Colorado experiment because the gravity data, geometric coordinates and GPS/leveling validation data are provided by NGS in the tide-free system. If everything is consistent, this should not influence the comparison results
Conversion of coefficient $C_{20}$ $\underline{C}_{20}^{TF} = \underline{C}_{20}^{ZT} + 3.11080 \cdot 10^{-8} \times 0.3/\sqrt{5}$	$\underline{C}_{20}^{TF}$ and $\underline{C}_{20}^{ZT}$ are the second-degree coefficients of the GGM in the tide-free and zero-tide system, respectively. For the Colorado computation, $C_{20}$ has to be expressed in the tide-free system
<i>First-degree terms</i>	
Coefficients: $C_1 = C_{11} = S_{11} = 0$	The disturbing potential $T$ is given by (cf. Equation 2–170, Heiskanen and Moritz, 1967):
Disturbing potential: $T_1(\theta, \lambda) = 0$	$T(\theta, \lambda) = T_0 + T_1(\theta, \lambda) + \sum_{n=2}^{\infty} T_n(\theta, \lambda)$ The first-degree terms are assumed to be zero to align the Earth's center of masses with the origin of the International Terrestrial Reference System (ITRS); i.e., the geometric coordinate system
<i>Zero-degree term</i>	
Disturbing potential: $T_0 = \frac{GM_{\text{GGM}} - GM_{\text{GRS80}}}{r_P}$	The zero-degree term $T_0$ must include the difference between Earth's and reference ellipsoid's $GM$ constant (cf. Equation 2–172, Heiskanen and Moritz, 1967). $r_P$ is the geocentric radial distance of the computation point $P$
Height anomaly*: $\zeta_0 = \frac{GM_{\text{GGM}} - GM_{\text{GRS80}}}{r_P \gamma_Q} - \frac{W_0 - U_0}{\gamma_Q}$	For the height anomaly ( $\zeta$ ) and the geoid undulation ( $N$ ), in addition to the difference between the two $GM$ values, the difference between the IHR reference potential $W_0$ value and the potential $U_0$ on the reference ellipsoid must be considered. It is recommended to compute the (quasi)geoid starting with $d/o = 2$ and then add the corresponding zero-degree term $\zeta_0$ or $N_0$
Geoid undulation*: $N_0 = \frac{GM_{\text{GGM}} - GM_{\text{GRS80}}}{r_{P_0} \gamma_{Q_0}} - \frac{W_0 - U_0}{\gamma_Q}$	

\*P is the computation point on the Earth's surface, Q is the projection of P along the normal plumb line on the telluroid, P<sub>0</sub> is the projection of P along the real plumb line on the geoid, and Q<sub>0</sub> is the projection of P<sub>0</sub> on the ellipsoid


## References

- Abd-Elmotaal H, Kühtreiber N (2003) Geoid determination using adapted reference field, seismic moho depths and variable density contrast. *J Geod* 77:77–85. <https://doi.org/10.1007/s00190-02-0300-7>
- Abd-Elmotaal H, Kühtreiber N (2021) Direct harmonic analysis for the ellipsoidal topographic potential with global and local validation. *Surv Geophys* 42:159–176. <https://doi.org/10.1007/s10712-020-09614-4>
- Ågren J, Ellmann A (2019) Report of the Sub-commission 2.2: Methodology for Geoid and Physical Height Systems, Reports 2015–2019 of the International Association of Geodesy (IAG), *Travaux de l'AIG Vol. 41*. Commission 2:33–38
- Ågren J, Sjöberg LE, Kiamehr R (2009) The new gravimetric quasigeoid model KTH08 over Sweden. *J Appl Geodesy* 3(3):1

- Ahlgren K, Wang YM, Li X, and Youngman M (2018) Towards a More Consistent Geoid Model for North America. FIG Congress 2018 Proceedings, Istanbul, Turkey
- Claessens SJ, Filmer MS (2020) Towards an International Height Reference System: insights from the Colorado experiment using AUSGeoid computation methods. *J Geod* 94:52. <https://doi.org/10.1007/s00190-020-01379-3>
- Damiani TM, Youngman M, and Johnson J (2017) GRAV-D General Airborne Gravity Data User Manual, GRAV-D Airborne Data Release User Manual v2.1. [https://geodesy.noaa.gov/GRAV-D/data/NGS\\_GRAV-D\\_General\\_Airborne\\_Gravity\\_Data\\_User\\_Manual\\_v2.1.pdf](https://geodesy.noaa.gov/GRAV-D/data/NGS_GRAV-D_General_Airborne_Gravity_Data_User_Manual_v2.1.pdf)
- Drewes H, Kuglitsch F, Ádám J, Rózsa S (2016) Geodesist's Handbook. *J Geod* 90:907. <https://doi.org/10.1007/s00190-016-0948-z>
- Flury J, Rummel R (2009) On the geoid–quasigeoid separation in mountain areas. *J Geod* 83:829–847. <https://doi.org/10.1007/s00190-009-0302-9>
- Forsberg R, Featherstone WE (1998) Geoids and cap sizes. In: *Geodesy on the Move - gravity, geoid, geodynamics and Antarctica*, Proceedings IAG scientific assembly, Rio de Janeiro, Sep 3–9, in: Forsberg, Feissel and Dietrich (eds.), IAG symposia 119, pp. 194–200, Springer Verlag
- Forsberg R (1987) A new covariance model for inertial gravimetry and gradiometry. *J. Geoph. Res* 92:1305–1310
- Forsberg R, Tscherning CC (1981) The use of height data in gravity field approximation by collocation. *J Geophys Res* 86(B9):7843–7854
- Grigoriadis VN, Vergos GS, Barzaghi R et al (2021) Collocation and FFT-based geoid estimation within the Colorado 1 cm geoid experiment. *J Geod* 95:52. <https://doi.org/10.1007/s00190-021-01507-7>
- Heck B (2011) A Brovar-type solution of the fixed geodetic boundary-value problem. *Stud Geophys Geod* 55:441–454. <https://doi.org/10.1007/s11200-011-0025-2>
- Heiskanen W, Moritz H (1967) *Physical geodesy*. Freeman, San Francisco
- Hirt C, Kuhn M, Claessens S, Pail R, Seitz K, Gruber T (2014) Study of the Earth's short scale gravity field using the ERTM2160 gravity model. *Comput Geosci* 73:71–80. <https://doi.org/10.1016/j.cageo.2014.09.001>
- Hofmann-Wellenhof B, Moritz H (2005) *Physical geodesy*. Springer, Wien New York
- Huang J, Wang YM (2019) Report of Joint Study Group 0.15: Regional geoid/quasigeoid modelling – theoretical framework for the sub-centimetre, Reports 2015–2019 of the International Association of Geodesy (IAG), *Travaux de l'AIG Vol. 41*, Inter-Commission Committee in Theory, pp 40–45
- Huang J, Véronneau M (2013) Canadian gravimetric geoid model 2010. *J Geod* 87:771–790. <https://doi.org/10.1007/s00190-013-0645-0>
- Ihde J, Sánchez L, Barzaghi R, Drewes H, Foerste C, Gruber T, Liesch G, Marti U, Pail R, Sideris M (2017) Definition and proposed realization of the International Height Reference System (IHR). *Surv Geophys* 38(3):549–570. <https://doi.org/10.1007/s10712-017-9409-3>
- Işık MS, Erol B, Erol S, Sakil FF (2021) High-resolution geoid modeling using least squares modification of Stokes and Hotine formulas in Colorado. *J Geod* 95:49. <https://doi.org/10.1007/s00190-021-01501-z>
- Jiang T, Dang YM, Zhang CY (2020) Gravimetric geoid modeling from the combination of satellite gravity model, terrestrial and airborne gravity data: a case study in the mountainous area, Colorado. *Earth, Planets and Space* 72:189. <https://doi.org/10.1186/s40623-020-01287-y>
- Jarvis A, Reuter HI, Nelson A, and Guevara E (2008) Hole-filled SRTM for the globe Version 4, available from the CGIAR-CSI SRTM 90m Database (<http://srtm.csi.cgiar.org>).
- Koch KR, Pope AJ (1972) Uniqueness and existence for the geodetic boundary value problem using the known surface of the earth. *Bull Géod* 46:467–476
- Liu Q, Schmidt M, Sánchez L, Willberg M (2020) Regional gravity field refinement for (quasi-) geoid determination based on spherical radial basis functions in Colorado. *J Geod*. <https://doi.org/10.1007/s00190-020-01431-2>
- Mayer-Gürr T, Kvas A, Klinger B, Rieser D, Zehentner N (2015) The new combined satellite gravity field only model GOCO05s. *Geophysical Research Abstracts*, vol 17, EGU2015–12364. EGU General Assembly 2013, Wien, Austria
- Matsuo K and Forsberg R (2021) Gravimetric geoid and quasigeoid computation over Colorado based on the Remove–Compute–Restore Stokes–Helmert scheme, submitted to *J Geod*, Special Issue on Reference Systems in Physical Geodesy
- Molodensky MS, Eremeev VF, Yurkina MI (1962) Methods for study of the external gravitational field and figure of the earth, Transl. from Russian (1960) Israel Program for Scientific Transl., Jerusalem
- Moritz H (2000) Geodetic Reference System 1980. *J Geod* 74(128–133):2000. <https://doi.org/10.1007/s001900050278>
- Moritz H (1980) *Advanced Physical Geodesy*. Wichmann Herbert Wichmann Verlag, Karlsruhe
- Pail R, Fecher T, Barnes D, Factor JF, Holmes SA, Gruber T, Zingerle P (2018) Short note: the experimental geopotential model XGM2016. *J Geod* 92:443–451. <https://doi.org/10.1007/s00190-017-1070-6>
- Pail R, Fecher T, Barnes D, Factor J, Holmes S, Gruber T, Zingerle P (2017) The experimental gravity field model XGM2016. GFZ Data Services. <https://doi.org/10.5880/icgem.2017.003>
- Rebischung P, Griffiths J, Ray J et al (2012) IGS08: the IGS realization of ITRF2008. *GPS Solut* 16:483–494. <https://doi.org/10.1007/s10291-011-0248-2>
- Reguzzoni M, Carrion D, De Gaetani CI, Albertella A, Rossi L, Sona G, Batsukh K, Toro Herrera JF, Elger K, Barzaghi R, Sansó F (2021) Open access to regional geoid models: the International Service for the Geoid. *Earth System Science Data* 13:1653–1666. <https://doi.org/10.5194/essd-13-1653-2021>
- Rexer M, Hirt C, Claessens S, Tenzer R (2016) Layer-Based Modelling of the Earth's Gravitational Potential up to 10-km Scale in Spherical Harmonics in Spherical and Ellipsoidal Approximation. *Surv in Geophy* 37:1035–1074. <https://doi.org/10.1007/s10712-016-9382-2>
- Ries JC, Fanes RJ, Shum CK, Watkins MM (1992) Progress in the determination of the gravitational coefficient of the Earth. *Geophys Res Lett* 19(6):529–531. <https://doi.org/10.1029/92GL00259>
- Sánchez L, Ågren J, Huang J, Wang YM, Mäkinen J, Pail R, Barzaghi R, Vergos GS, Ahlgren K, Liu Q (2021) Strategy for the realisation of the International Height Reference System (IHR). *J Geodesy* 95(3):1. <https://doi.org/10.1007/s00190-021-01481-0>
- Sánchez L, Barzaghi R (2020) Activities and plans of the GGOS Focus Area Unified Height System, EGU General Assembly 2020, EGU2020-8625, <https://doi.org/10.5194/egusphere-egu2020-8625>
- Sánchez L (2019) Report of the GGOS Focus Area “Unified Height System” and the Joint Working Group 0.1.2: Strategy for the Realization of the International Height Reference System (IHR), Reports 2015–2019 of the International Association of Geodesy (IAG), *Travaux de l'AIG Vol. 41*, Global Geodetic Observing System (GGOS), pp 42–51
- Sánchez L, Ågren J, Huang J, Wang YM, Forsberg R (2018) Basic agreements for the computation of station potential values as IHR coordinates, geoid undulations and height anomalies within the Colorado 1-cm geoid experiment. Version 0.5, October 30, 2018
- Sánchez L, Čunderlík R, Dayoub N, Mikula K, Minarechová Z, Šíma Z, Vatr V, Vojtíšková M (2016) A conventional value for the geoid

- reference potential W0. *J Geod* 90:815–835. <https://doi.org/10.1007/s00190-016-0913-x>
- Sjöberg LE (2010) A strict formula for geoid-to-quasigeoid separation. *J Geod* (2010) 84: 699. <https://doi.org/10.1007/s00190-010-0407-1>
- Sjöberg LE (2003) A computational scheme to model the geoid by the modified Stokes formula without gravity reductions. *J Geod* 77:423–432. <https://doi.org/10.1007/s00190-003-0338-1>
- Sjöberg LE (1984) Least-Squares modification of Stokes' and Venning–Meinez' formula by accounting for truncation and potential coefficients errors. *Manuscr Geod* 9:209–229
- Sjöberg LE (1981) Least squares combination of satellite and terrestrial data in physical geodesy. *Ann Géophys* 37(1):25–30
- Sjöberg LE (1980) Least squares combination of satellite harmonics, and integral formulas in physical Geodesy. *Gerlands Beiträge Zur Geophysik* 89(5):371–377
- Smith DA, Holmes SA, Li X, Guillaume S, Wang YM, Bürki B, Roman DR, Damiani T (2013) Confirming regional 1 cm differential geoid accuracy from airborne gravimetry: the Geoid Slope Validation Survey of 2011. *J Geod* 87:885–907
- Tscherning CC (1984) The Geodesist's Handbook, *Bull Géod* 58(3):1
- Tscherning, CC and Rapp RH (1974) Closed covariance expressions for gravity anomalies, geoid undulations and deflections of the vertical implied by anomaly degree variance models. Department of Geodetic Science, Report No. 208, The Ohio State University
- Vaniček P, Martinec Z (1994) Stokes-Helmert scheme for the evaluation of a precise geoid. *Manus Geod* 19(2):119–128
- van Westrum D, Ahlgren K, Hirt C, Guillaume S (2021) A Geoid Slope Validation Survey (2017) in the rugged terrain of Colorado, USA. *J Geod* 95:9. <https://doi.org/10.1007/s00190-020-01463-8>
- Varga M, Pitoňák M, Novák P, Bašić T (2021) Contribution of GRAV-D airborne gravity to improvement of regional gravimetric geoid modelling in Colorado, USA. *J Geod* 95:53. <https://doi.org/10.1007/s00190-021-01494-9>
- Wang YM, Véronneau M, Huang J, Ahlgren K, Krcmaric J, Li X, Avalos D (2021) On the accurate computation of the geoid-quasigeoid separation in a mountainous region—a case study in Colorado with a full extension to the experimental geoid region. *J Geodetic Sci* (submitted)
- Wang YM, Li X, Ahlgren K, Krcmaric J (2020) Colorado geoid modeling at the US National Geodetic Survey. *J Geod* 94:106. <https://doi.org/10.1007/s00190-020-01429-w>
- Wang YM, Forsberg R (2019) Report of the Joint Working Group 2.2.2: The 1 cm geoid experiment, Reports 2015-2019 of the International Association of Geodesy (IAG), *Travaux de l'AIG Vol. 41, Commission 2*, pp 56–58
- Wang YM, Holmes S, Li X, and Ahlgren K (2017a) NGS Annual Experimental Geoid Models – xGEOID17: What is new and the results, IAG-IASPEI, Kobe, Japan July 30 - August 5, 2017.
- Wang YM, Becker C, Mader G et al (2017b) The Geoid Slope Validation Survey 2014 and GRAV-D airborne gravity enhanced geoid comparison results in Iowa. *J Geod* 91:1261. <https://doi.org/10.1007/s00190-017-1022-1>
- Willberg M, Zingerle P, Pail R (2020) Integration of airborne gravimetry data filtering into residual least-squares collocation: example from the 1 cm geoid experiment. *J Geod* 94:75. <https://doi.org/10.1007/s00190-020-01396-2>
- Willberg M, Zingerle P, Pail R (2019) Residual least-squares collocation: use of covariance matrices from high-resolution global geopotential models. *J Geod* 93:1739–1757. <https://doi.org/10.1007/s00190-019-01279-1>
- Zilkoski DB, Richards JH, Young GM (1992) Results of the general adjustment of the North American Vertical Datum of 1988. *Surv Land Inf Syst* 52(3):133–149

## Author and Affiliations

Yan Ming Wang<sup>1</sup>  · Laura Sánchez<sup>2</sup> · Jonas Ågren<sup>3,4,5</sup> · Jianliang Huang<sup>6</sup> · René Forsberg<sup>7</sup> · Hussein A. Abd-Elmotaal<sup>8</sup> · Kevin Ahlgren<sup>1</sup> · Riccardo Barzaghi<sup>9</sup> · Tomislav Bašić<sup>10</sup> · Daniela Carrion<sup>9</sup> · Sten Claessens<sup>11</sup> · Bihter Erol<sup>12</sup> · Serdar Erol<sup>12</sup> · Mick Filmer<sup>11</sup> · Vassilios N. Grigoriadis<sup>13</sup> · Mustafa Serkan Isik<sup>12</sup> · Tao Jiang<sup>14</sup> · Öykü Koç<sup>12</sup> · Jordan Krčmaric<sup>1</sup> · Xiaopeng Li<sup>1</sup> · Qing Liu<sup>2</sup> · Koji Matsuo<sup>15</sup> · Dimitris A. Natsiopoulou<sup>13</sup> · Pavel Novák<sup>16</sup> · Roland Pail<sup>17</sup> · Martin Pitoňák<sup>16</sup> · Michael Schmidt<sup>2</sup> · Matej Varga<sup>18</sup> · Georgios S. Vergos<sup>13</sup> · Marc Véronneau<sup>6</sup> · Martin Willberg<sup>17</sup> · Philipp Zingerle<sup>17</sup>

- <sup>1</sup> National Geodetic Survey, 1315 East-West Highway, Silver Spring, MD 20910-3282, USA
- <sup>2</sup> Deutsches Geodätisches Forschungsinstitut, Technical University of Munich, Arcisstr. 21, 80333 Munich, Germany
- <sup>3</sup> Department of Computer and Geospatial Sciences, University of Gävle, 80176 Gävle, Sweden
- <sup>4</sup> Lantmäteriet, Swedish Mapping, Cadastral and Land Registration Authority, 80182 Gävle, Sweden
- <sup>5</sup> KTH Royal Institute of Technology, 10044 Stockholm, Sweden
- <sup>6</sup> Canadian Geodetic Survey, Surveyor General Branch, Natural Resources Canada, 588 Booth Street, Ottawa, ON K1A 0Y7, Canada
- <sup>7</sup> Technical University of Denmark, Elektrovej, Building 327, 2800 Kgs. Lyngby, Denmark
- <sup>8</sup> Civil Engineering Department, Faculty of Engineering, Minia University, Minia 61111, Egypt
- <sup>9</sup> Department of Civil and Environmental Engineering, Politecnico Di Milano, Piazza Leonardo da Vinci, 32, 20133 Milan, Italy
- <sup>10</sup> Faculty of Geodesy, University of Zagreb, Kačićeva 26, 10000 Zagreb, Republic of Croatia
- <sup>11</sup> School of Earth and Planetary Sciences and The Institute for Geoscience Research, Curtin University, GPO Box U1987, Perth, WA 6845, Australia
- <sup>12</sup> Geomatics Engineering Department, Civil Engineering Faculty, Istanbul Technical University, Ayazağa Campus, 34469 Maslak/Istanbul, Turkey
- <sup>13</sup> Laboratory of Gravity Field Research and Applications, Department of Geodesy and Surveying, Aristotle University of Thessaloniki, University Box 440, 54124 Thessaloniki, Greece
- <sup>14</sup> Chinese Academy of Surveying and Mapping, 28 Lianhuachi West Road, Beijing 100830, China
- <sup>15</sup> Geospatial Information Authority of Japan, 1, Kitasato, Tsukuba 305-0811, Japan
- <sup>16</sup> New Technologies for the Information Society, Faculty of Applied Sciences, University of West Bohemia, Technická 8, 30614 Pilsen, Czech Republic
- <sup>17</sup> Institute of Astronomical and Physical Geodesy, Technical University of Munich, Arcisstr. 21, 80333 Munich, Germany
- <sup>18</sup> Institute of Geodesy and Photogrammetry, GSEG, ETH Zürich, Stefano-Francini-Platz 5, 8093 Zurich, Switzerland